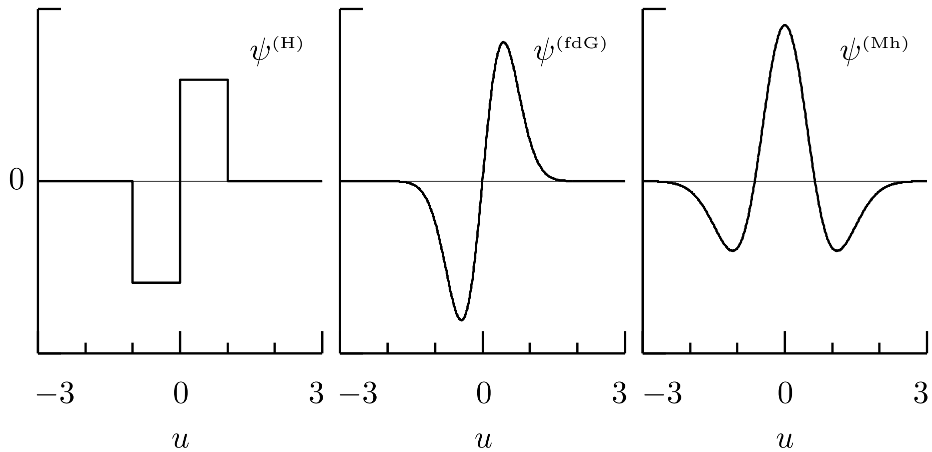

Figure 1. Three wavelets. From left to right, we have one version of the Haar wavelet; a wavelet that is related to the first derivative of the Gaussian probability density function (PDF); and the Mexican hat wavelet, which is related to the second derivative of the Gaussian PDF.

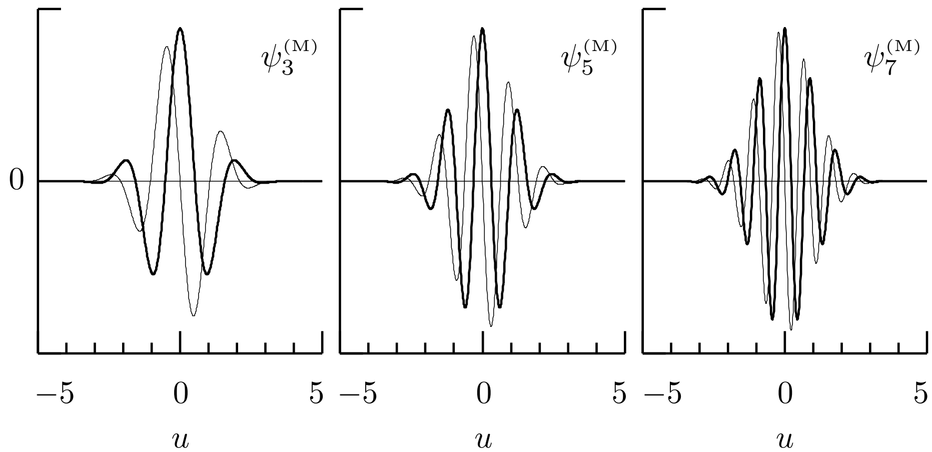

Figure 2. Three Morlet wavelets $\psi_{\omega_0}^{(M)}(\cdot)$. These wavelets are complex-valued, so their real and imaginary parts are plotted using, respectively, thick and thin curves. The parameter ω_0 controls the frequency of the complex exponential that is then modulated by a function whose shape is dictated by the standard Gaussian PDF. As ω_0 increases from 3 to 7, the number of oscillations within the effective width of the Gaussian PDF increases.

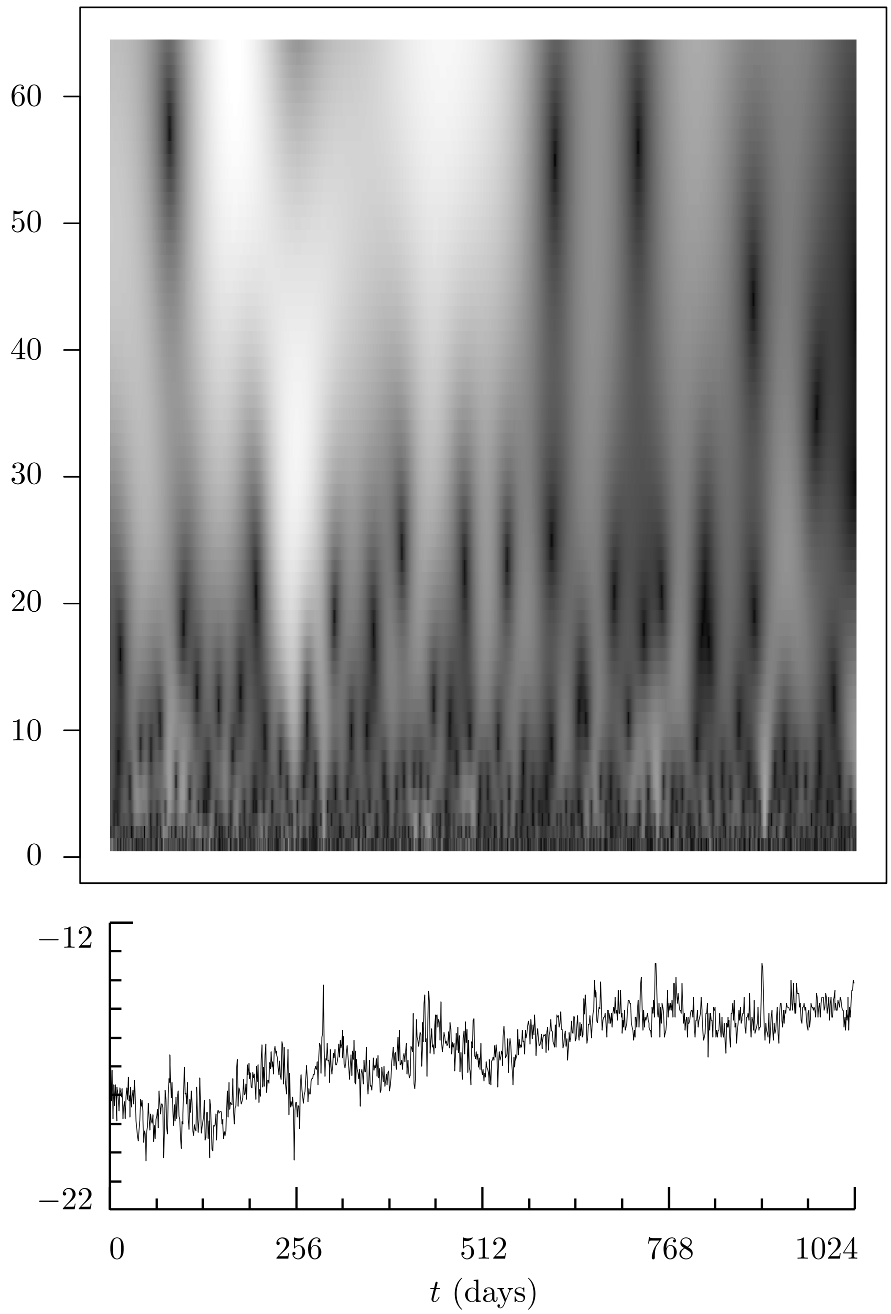

Figure 3. Average daily fractional frequency deviates for cesium beam atomic clock 571 (bottom plot) and its Mexican hat CWT. The fractional frequency deviates are recorded in parts in 10^{13} (a deviation of -15 parts in 10^{13} means that clock 571 lost about 129.6 billionths of a second in one day with respect to the US Naval Observatory master clock to which it was being compared). The vertical axis of the CWT plot is scale (ranging from 1 to 64 days), while the horizontal axis is the same as on the lower plot. The CWT plot is grey-scaled coded so that large magnitudes correspond to bright spots (regions where the plot is dark indicate scales and days at which the clock performed well).

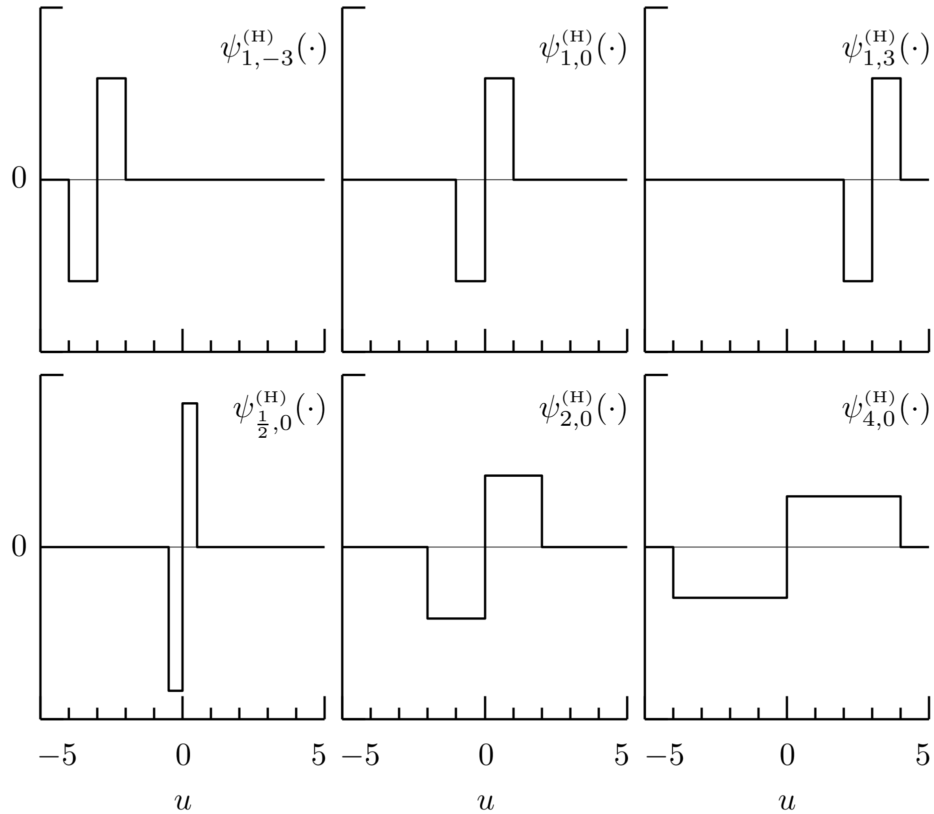

Figure 4. Shifted and rescaled versions of the Haar wavelet $\psi^{(\mathrm{H})}(\cdot)$. The plots above show $\psi^{(\mathrm{H})}_{\lambda,t}(\cdot)$, which can be used to measure how much adjacent averages of a signal $x(\cdot)$ over a scale of length λ change at time t. The top row of plots shows the effect of keeping λ fixed at unity while t is varied; in the bottom row t is fixed at zero while λ is varied.

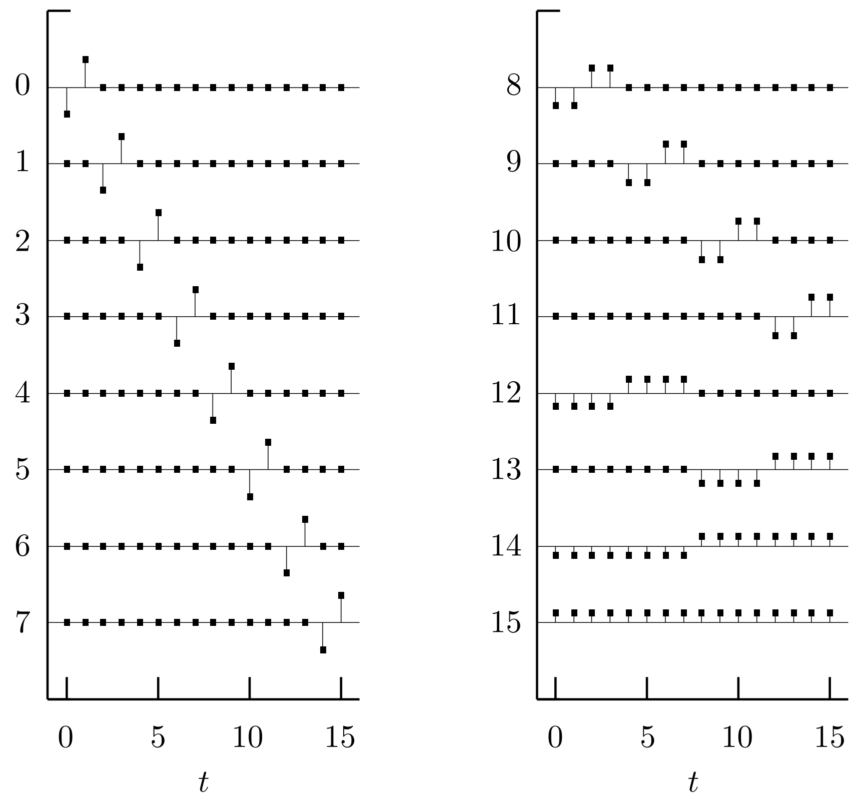

Figure 5. Row vectors $\mathcal{W}_{n\bullet}^T$ of the discrete wavelet transform matrix $\mathcal{W}$ based on the Haar wavelet for $N = 16$ and $n = 0$ to 7 (top to bottom on left plot) and $n = 8$ to 15 (right plot).

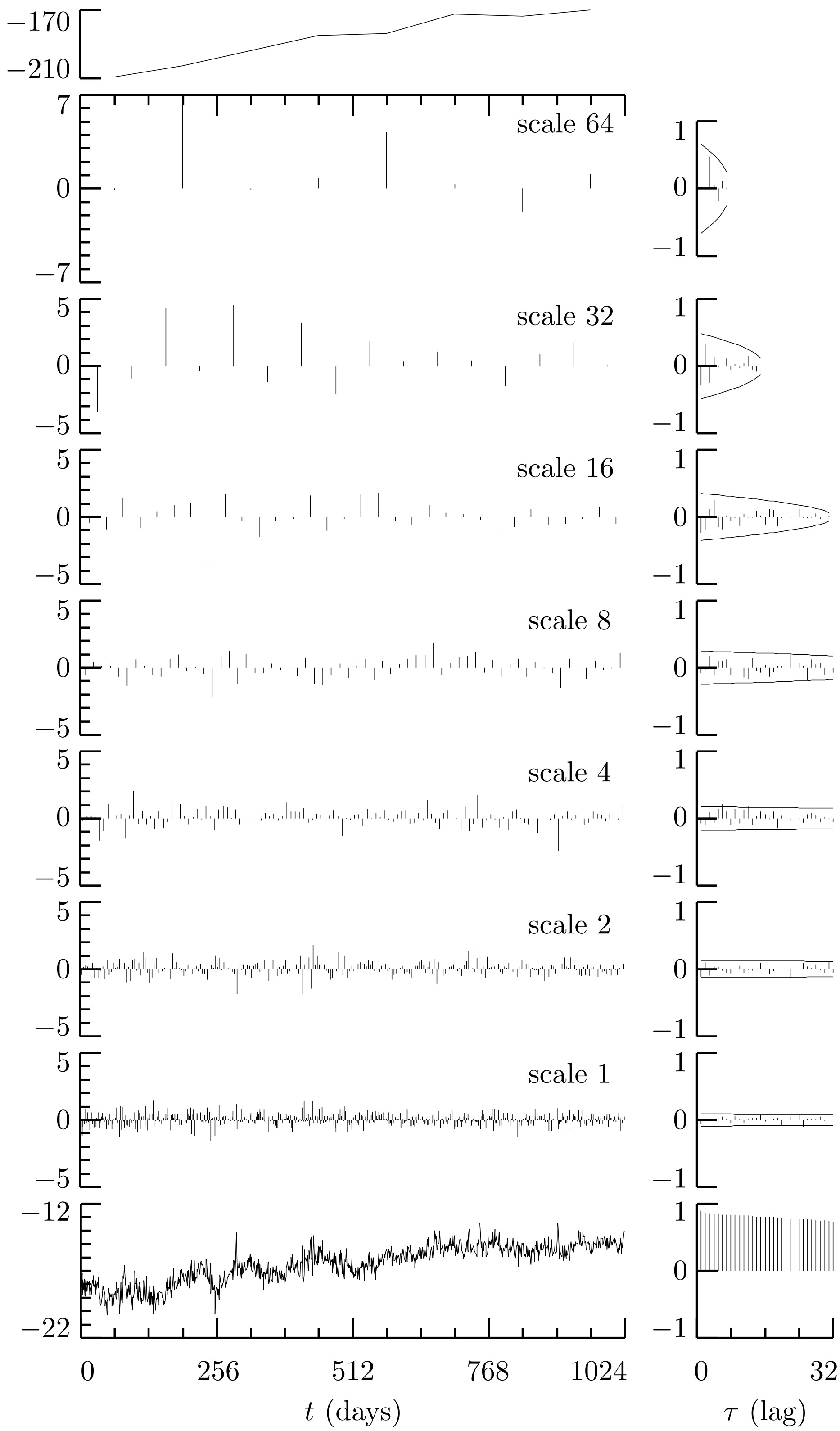

Figure 6. Haar DWT coefficients for clock 571 and sample autocorrelation sequences (ACSs).

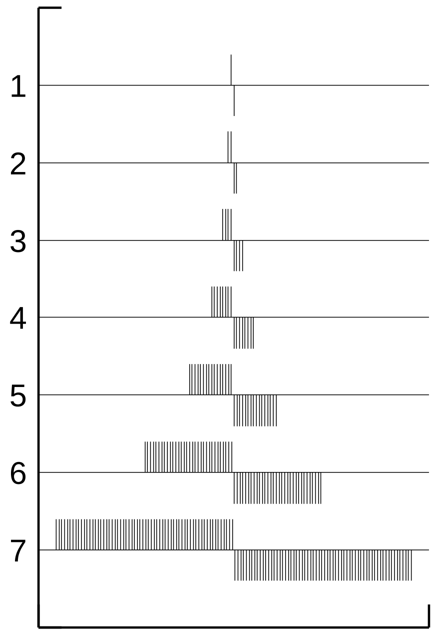

Figure 7. Haar wavelet filters for scales $\tau_j = 2^{j-1}$, $j = 1, 2, \ldots, 7$.

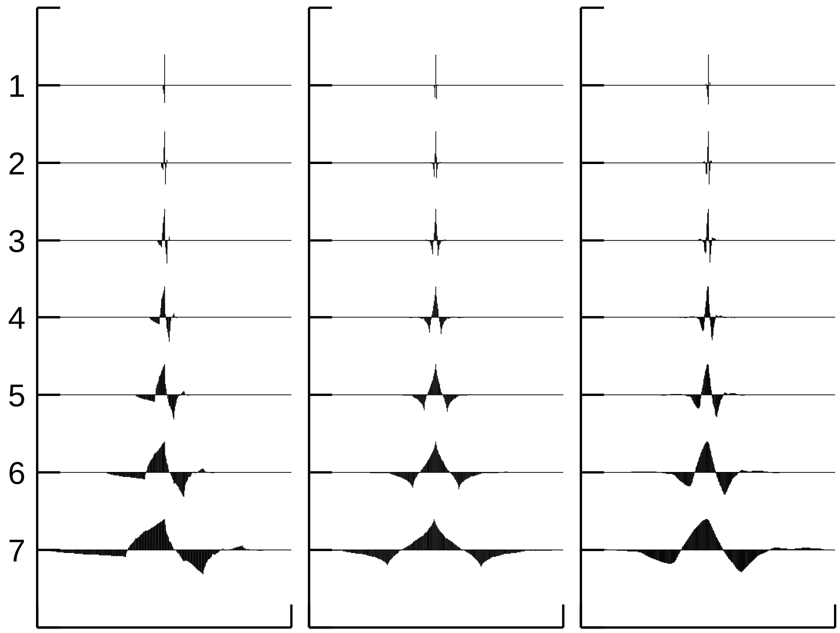

Figure 8. D(4), C(6) and LA(8) wavelet filters for scales $\tau_j = 2^{j-1}$, $j = 1, 2, \ldots, 7$.

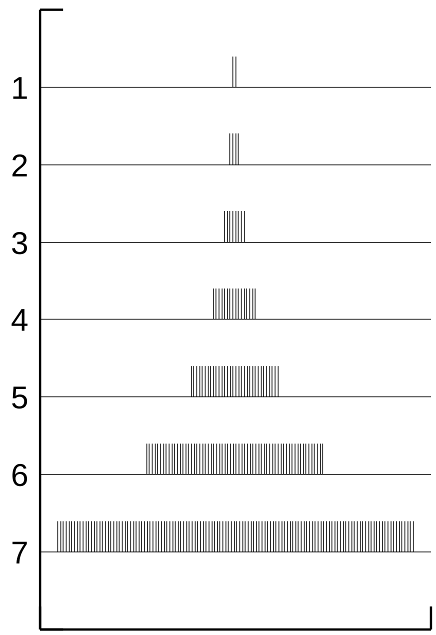

Figure 9. Haar scaling filters for scales $\lambda_{J_0} = 2^{J_0},\ J_0 = 1, 2, \ldots, 7$.

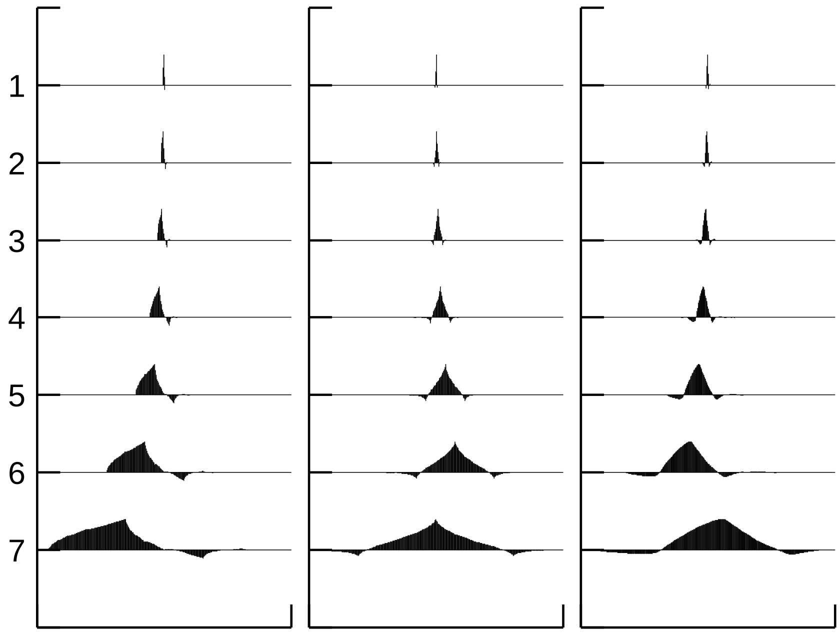

Figure 10. D(4), C(6) and LA(8) scaling filters for scales $\lambda_{J_0} = 2^{J_0},\ J_0 = 1, 2, \ldots, 7.$

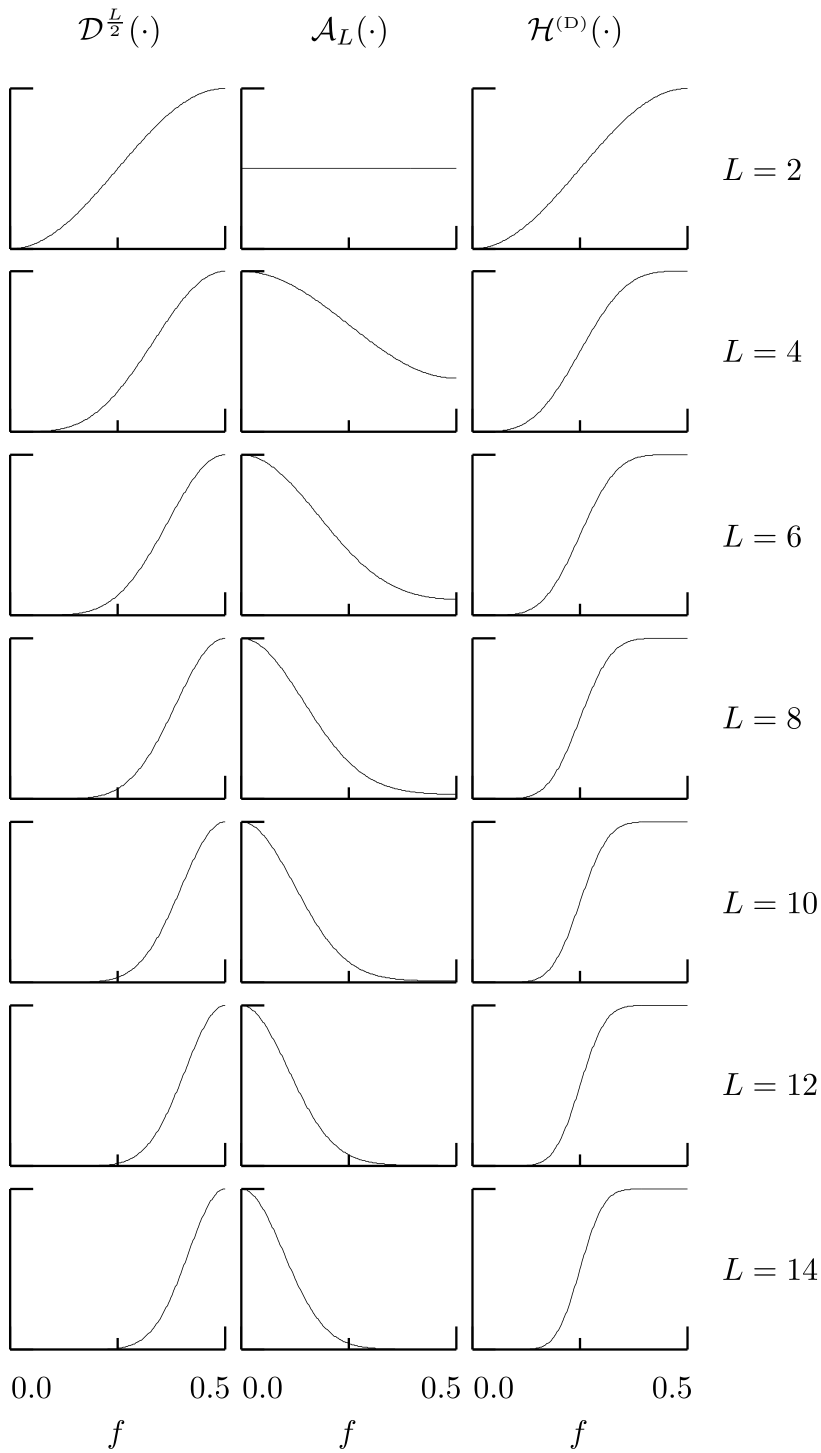

Figure 11. Squared gain functions $\mathcal{H}^{(\mathrm{D})}(\cdot)$ for Daubechies wavelet filters of widths $L = 2, 4, \ldots, 14$ (right-hand column). Each $\mathcal{H}^{(\mathrm{D})}(\cdot)$ is the product of two other squared gain functions, namely, $\mathcal{D}^{\frac{L}{2}}(\cdot)$ (left-hand column) and $\mathcal{A}_L(\cdot)$ (middle). The first corresponds to an $\frac{L}{2}$ order difference filter, while for $L \geq 4$ the second is associated with a weighted average (i.e., low-pass filter).

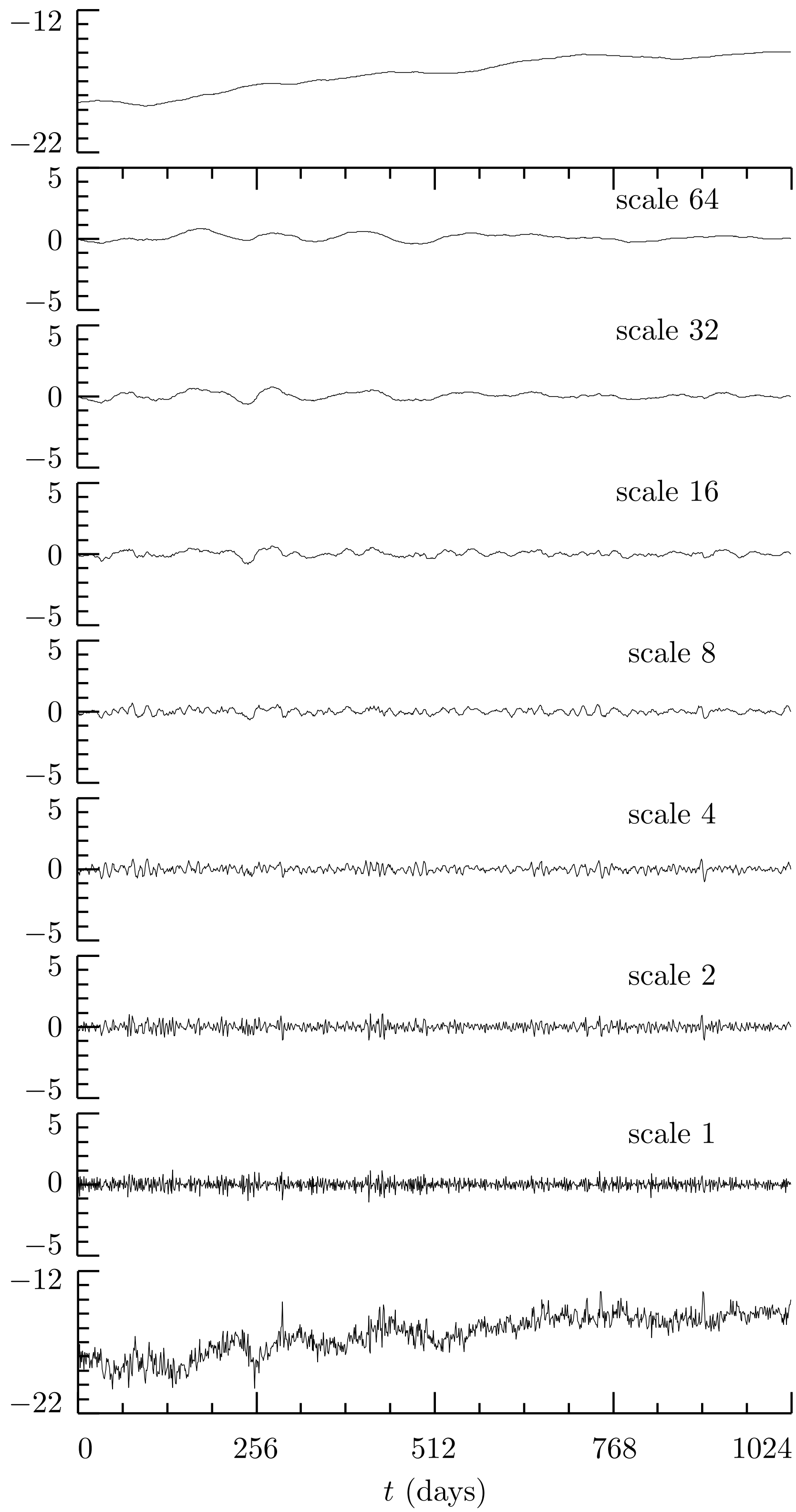

Figure 12. Haar MODWT coefficients for clock 571.

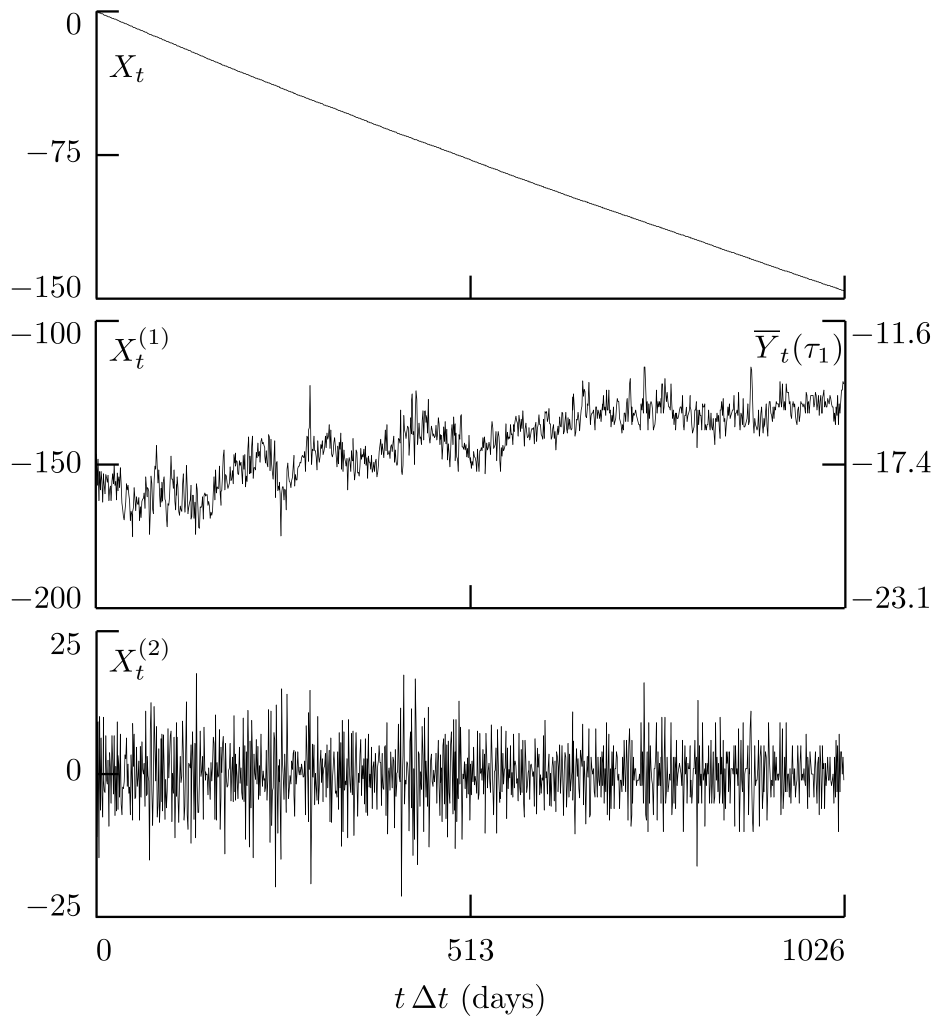

Figure 13. Plot of differences in time $\{X_t\}$ as kept by clock 571 (a cesium beam atomic clock) and as kept by the time scale UTC(USNO) maintained by the US Naval Observatory, Washington, DC (top plot); its first backward difference $\{X_t^{(1)}\}$ (middle); and its second backward difference $\{X_t^{(2)}\}$ (bottom). In the middle plot, $\overline{Y}_t(\tau_1)$ denotes the τ_1 average fractional frequency deviates (given in parts in 10^{13}) – these are proportional to $X_t^{(1)}$.

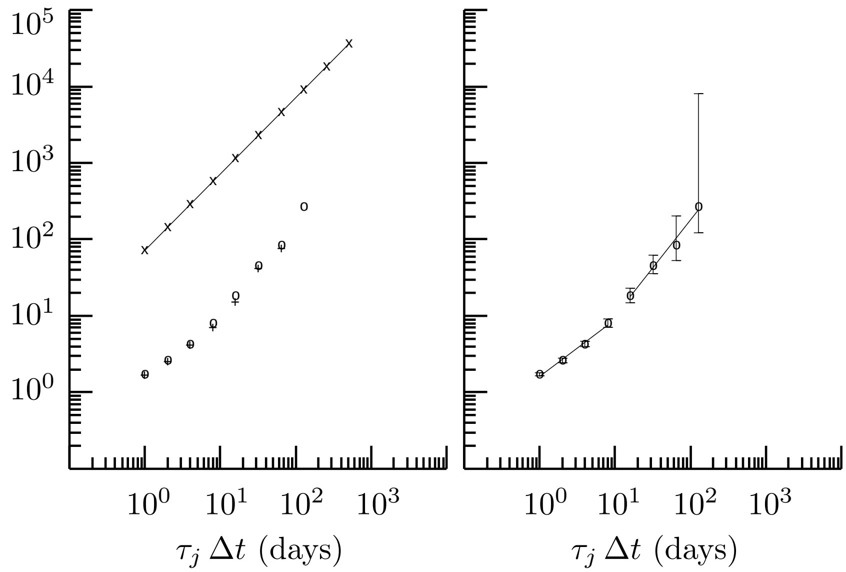

Figure 14. Square roots of wavelet variance estimates for atomic clock time differences $\{X_t\}$ based upon the unbiased MODWT estimator and the following wavelet filters: Haar (x's in left-hand plot, through which a least squares line has been fit), D(4) (circles in left- and right-hand plots) and D(6) (pluses in left-hand plot). The right-hand plot also shows 95% confidence intervals for the unknown wavelet variances.

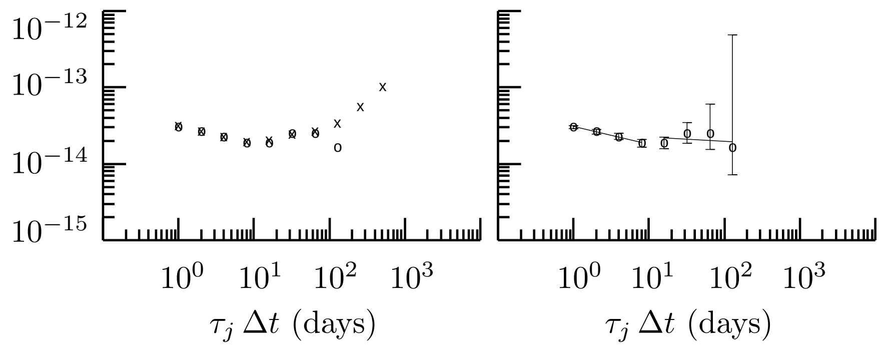

Figure 15. Square roots of wavelet variance estimates for atomic clock one day average fractional frequency deviates $\{\overline{Y}_t(\tau_1)\}$ based upon the unbiased MODWT estimator and the following wavelet filters: Haar (x's in left-hand plot) and D(4) (circles in left and right-hand plots).

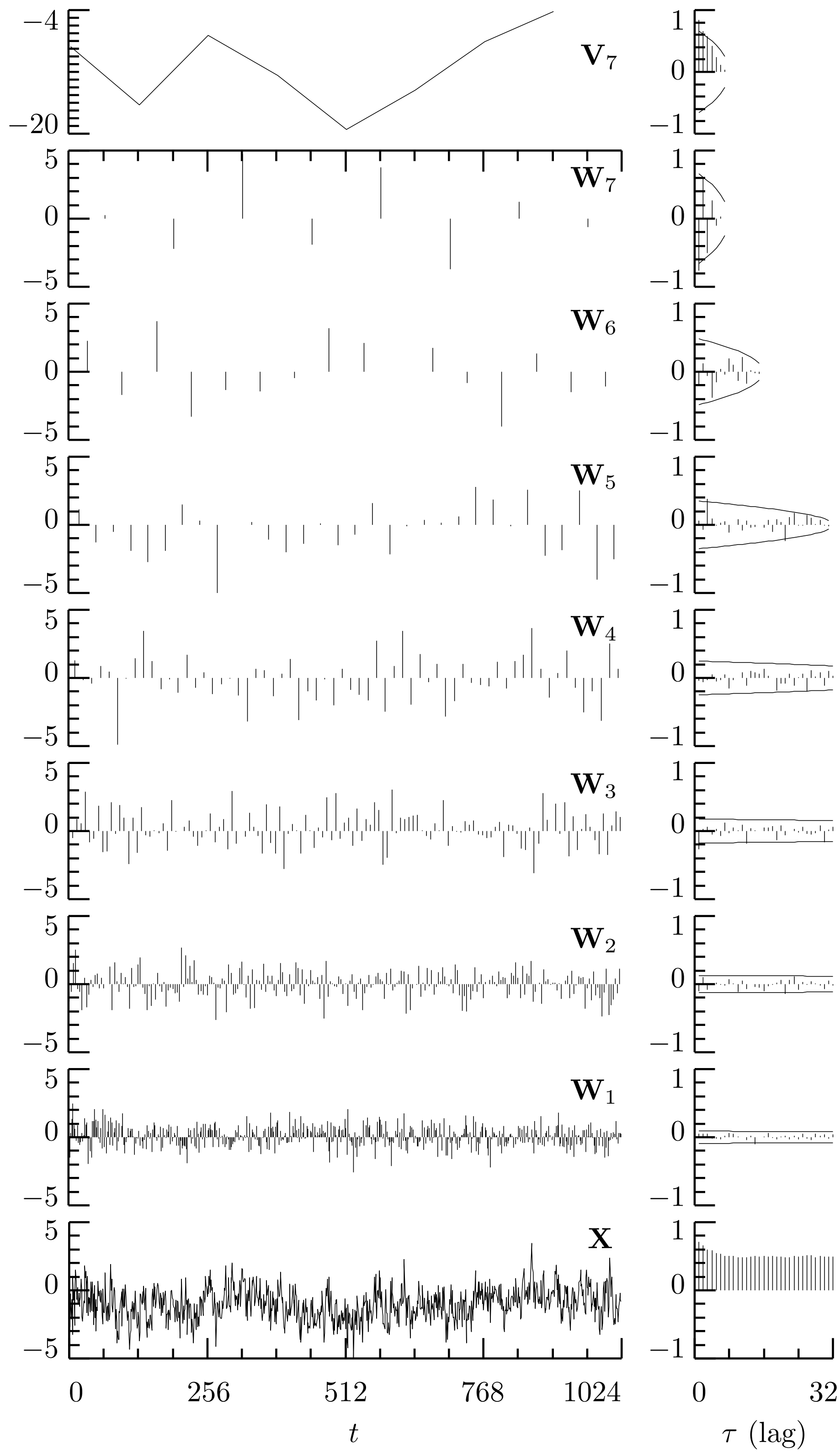

Figure 16. LA(8) DWT coefficients for simulated FD(0.4) time series and sample ACSs.

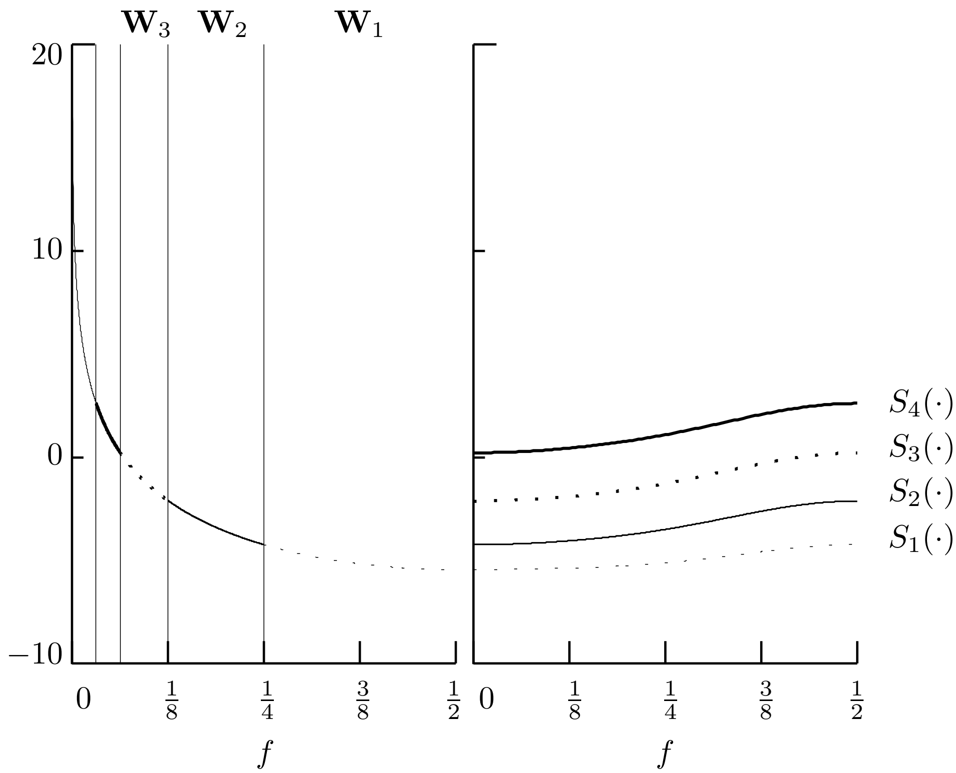

Figure 17. SDFs for an FD(0.4) process (left-hand plot) and for nonboundary LA(8) wavelet coefficients in $\mathbf{W}_1$, $\mathbf{W}_2$, $\mathbf{W}_3$ and $\mathbf{W}_4$ (right-hand). The vertical axis is in units of decibels (i.e., we plot $\log_{10}(S_X(f))$ versus f). The vertical lines in the left-hand plot denote the nominal pass-bands for the four $\mathbf{W}_j$.

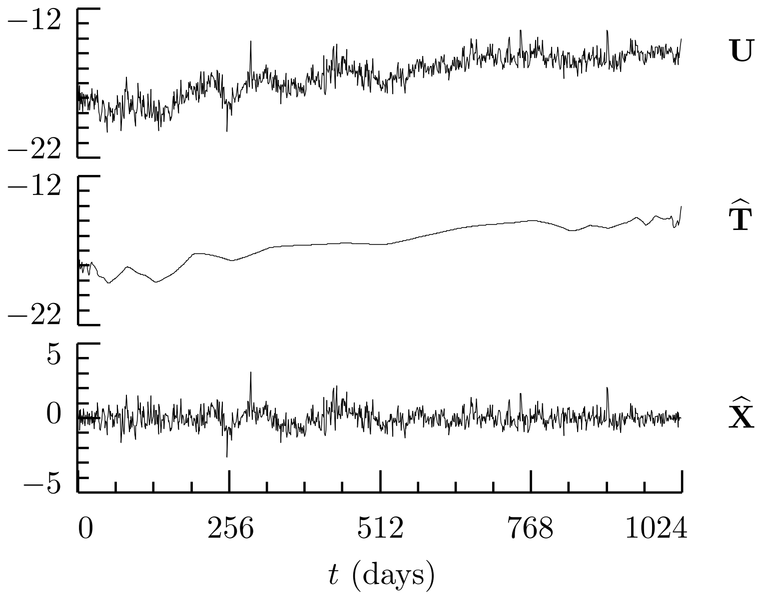

Figure 18. Wavelet-based decomposition of atomic clock fractional frequency deviates $\mathbf{U} = \overline{\mathbf{Y}}$ into an estimated trend $\widehat{\mathbf{T}}$ and residuals $\widehat{\mathbf{X}}$ about the trend. Here we used an LA(8) partial DWT of level $J_0 = 7$. Note that $\widehat{\mathbf{T}}$ has much more structure than a low order polynomial and in fact resembles the output from a variable bandwidth smoother: it is quite smooth near the middle of the series, but then becomes rougher in appearance toward the end points.

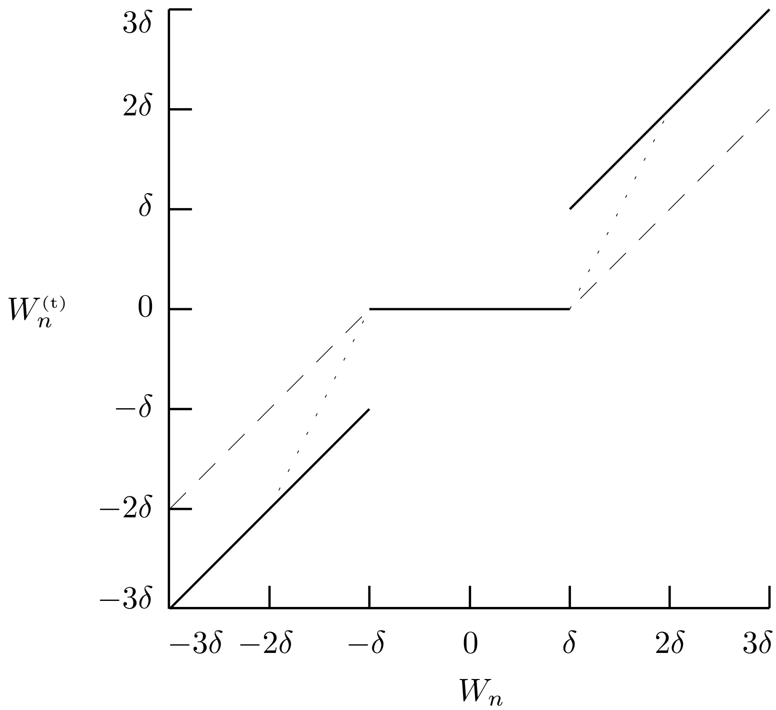

Figure 19. Mappings from W_n to $W_n^{(\mathrm{t})}$, where $W_n^{(\mathrm{t})}$ is either $W_n^{(\mathrm{ht})}$ for hard thresholding (solid lines), $W_n^{(\mathrm{st})}$ for soft thresholding (dashed lines), or $W_n^{(\mathrm{mt})}$ for mid thresholding (dotted lines). Note that the effect of all three thresholding schemes is the same when $-\delta \leq W_n \leq \delta$.

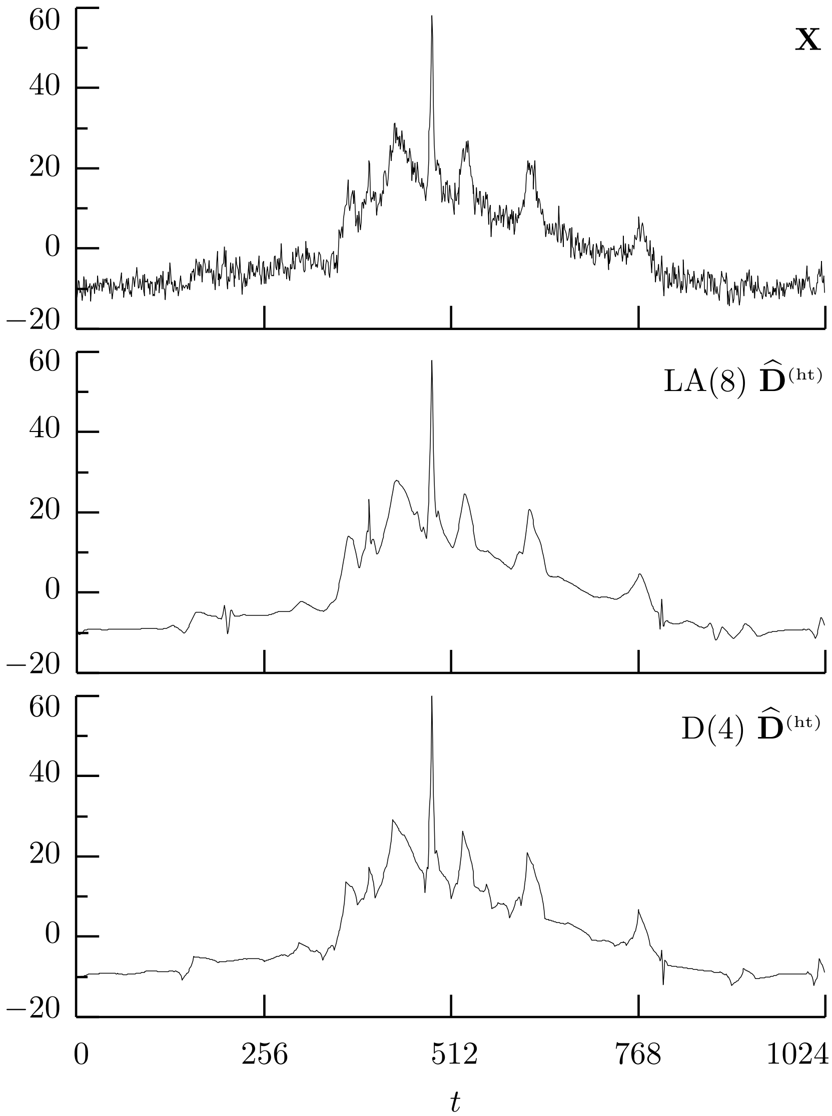

Figure 20. Nuclear magnetic resonance (NMR) spectrum (top plot), along with wavelet-based hard threshold signal estimates using the level $J_0 = 6$ partial LA(8) DWT (middle) and a similar D(4) DWT (bottom). In both cases, we determine the noise variance σ_ϵ^2 using the MAD standard deviation estimate $\hat{\sigma}_{(\mathrm{mad})}$, after which we set the universal threshold level $\hat{\delta}^{(\mathrm{u})} \equiv \sqrt{[2\hat{\sigma}^2_{(\mathrm{mad})} \log(N)]}$. This NMR spectrum was extracted from the public domain software package `WaveLab`, to which it was provided by Andrew Maudsley, Department of Radiology, University of California, San Francisco.